Proceedings of the
44th IEEE Conference on Decision and Control, and
the European Control Conference 2005
Seville, Spain, December 12-15, 2005

MoA15.2

Wake stabilization using POD Galerkin models with interpolated modes

OLIVER LEHMANN
MARK LUCHTENBURG
BERND R. NOACK
RUDIBERT KING

Berlin University of Technology
Straße des 17. Juni 135
D-10623 Berlin, Germany
Oliver.Lehmann@pi.tu-berlin.de

MAREK MORZYŃSKI

Institute of Combustion Engines
and Transportation
Poznań University of Technology
Ulica Piotrowo 3
PL 60-965 Poznań, Poland
Marek.Morzynski@put.poznan.pl

GILEAD TADMOR

Electrical & Computer
Engineering Department
Northeastern University
440 Dana Research Building
Boston, MA 02115, U.S.A.
Tadmor@ece.neu.edu

Abstract— **A principal challenge in the use of empirical proper orthogonal decomposition (POD) Galerkin models for feedback control design in fluid flow systems is their typical fragility and poor dynamic envelope. Closed loop performance and optimized sensor(s) location are significantly improved by use of interpolated POD modes from a succession of low dimensional models from sections of a controlled transient manifold. This strategy is demonstrated in the benchmark of stabilization of the wake flow behind a circular cylinder.**

I. INTRODUCTION

The complexity of fluid dynamics and related computational (CFD) models, is a major hindrance to model based feedback control [1]: Hardware architecture optimization, feedback design and real time implementation are prohibitively expensive with such models. Effective low-dimensional flow models are therefore essential enablers.

Empirical proper orthogonal decomposition (POD) Galerkin models (GMs), based on a Karhunen-Loève approximation of flow data [2], offer efficient low-dimensional flow representations. Yet for control applications, PODs suffer from fundamental deficiencies: Dynamic fragility away from the reference orbit and flow conditions is particularly detrimental in a context where transients occupy center stage. Other shortcomings include truncated energy dynamics and a difficulty to incorporate boundary actuation. This note follows a succession of studies, e.g. [3]–[19], aiming to develop tools that make empirical GMs useful for control design.

One basic observation is that any low dimensional flow model is necessarily restricted to a dynamic manifold, formed by targeted families of transients. The issue at hand is therefore an effective modeling of the dynamics in subspace neighborhoods of such manifolds. In some cases, reasonable representations of *natural* transients from an unstable steady flow to an attractor are feasible with modes from both the start and end operating conditions are used, along with mean flow correction [8]. When system identification tools are used to correct system coefficients, modes extracted from the attractor and mean flow changes alone may suffice [17]. The representation of *actuated* transient manifolds appears to be considerably more challenging. For example whereas 3 modes suffice to capture the essence of natural transients in the laminar cylinder wake flow, some 40 POD modes were used to capture the actuated transient manifold when optimal control was sought in the same system [20]. This dimension proliferation is needed for two reasons: To compensate for the gradual deformation of dominant modes along transients and to assure sufficiently accurate prediction of actuation effects.

Here we explore an alternative modeling approach for systems where local characteristics of expansion modes geometry and model structure are preserved at intermediate operating points. The idea is to interpolate a series of local, similarly structured expansions, as a substitute for the use of a single, higher order global model. We illustrate this approach by the ubiquitous benchmark of laminar vortex shedding suppression behind a cylinder [21]–[24]. In this benchmark, instead of a single, 40-dimensional global model, a succession of 3 dimensional, similarly structured models will be used, where the 2 modes representing the oscillatory vortex shedding are varied as the system traverses actuated transients. The advantage over the traditional POD model are demonstrated both with respect to achievable closed loop performance and when sensor locations are optimized, to assure even performance throughout the transient range, rather than in a narrow neighborhood of the natural attractor.
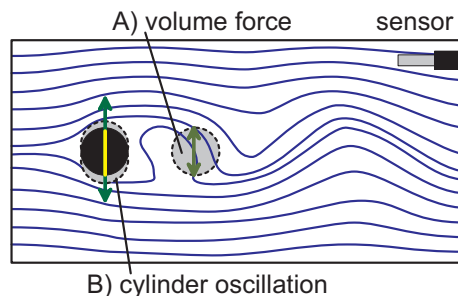

Fig. 1. A sketch of the actuated cylinder wake. The cylinder is represented by the black disk. The location of the volume-force actuator (A) is indicated by a grey circle. An alternative actuation is by transverse cylinder motion (B). Streamlines represent the natural flow. The figure includes a hot-wire anemometer at a typical experimental position. This sensor has been used in an observer-based control using a Galerkin model [9].

II. EMPIRICAL GALERKIN MODELS

Empirical Galerkin models are based on experimental data or a direct numerical simulation (DNS) of the non-dimensionalized, incompressible, actuated Navier-Stokes equation (NSE)

$$\partial_t \mathbf{u} + \nabla \cdot (\mathbf{uu}) = -\nabla p + \frac{1}{Re} \triangle \mathbf{u} + \epsilon \, \mathbf{g}, \quad \nabla \cdot \mathbf{u} = 0 \quad (1)$$

where $\mathbf{u}(\mathbf{x}, t)$ is the velocity field, p the pressure, and $\mathbf{g}(\mathbf{x})$ a volume force modulated by the control command $\epsilon(t)$. The Reynolds number $Re = UD/\nu$ is based on the non-dimensionalization scales of velocity U, length D and kinematic viscosity ν.
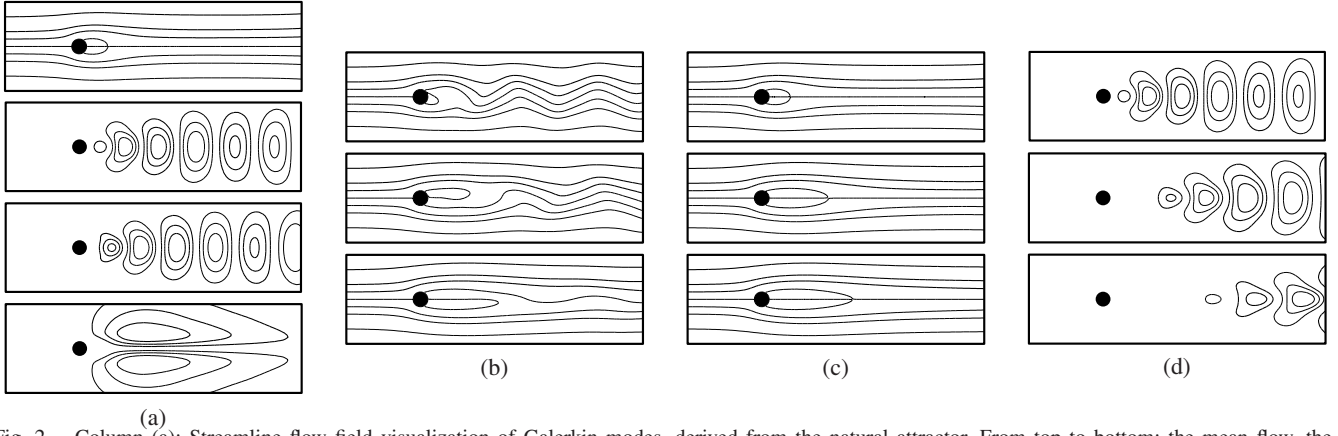
Fig. 2. Column (a): Streamline flow field visualization of Galerkin modes, derived from the natural attractor. From top to bottom: the mean flow, the first two POD modes resolving 95% of the fluctuation energy, and the shift mode. Each of the columns (b), (c) & (d) compares the natural flow (top), moderately forced (middle) and more aggressively forced (bottom) flows. (b): Snapshots of level curves of the flow field. (c): Averaged flows. (d): First POD mode.

A. Standard models

Having fixed a spatial flow domain Ω, velocity fields are embedded in the Hilbert space $\mathcal{L}_2(\Omega)$ with the inner product

$$(\mathbf{u}, \mathbf{v})_\Omega := \int_\Omega dV \, \mathbf{u} \cdot \mathbf{v}, \quad \mathbf{u}, \mathbf{v} \in \mathcal{L}_2(\Omega). \quad (2)$$

The Galerkin approximation of the flow is expressed by

$$\mathbf{u}^{[N]}(\mathbf{x}, t) = \sum_{i=0}^{N} a_i(t) \, \mathbf{u}_i(\mathbf{x}), \quad (3)$$

where the coefficients $a_i(t)$ capture time dependence, $\mathbf{u}_0$ is the time-averaged field (so that $a_0 \equiv 1$, by definition [3]), and $\mathbf{u}_i$, $i \geq 1$, are orthonormal POD modes [2] that minimize the averaged energy residual in (3), in the reference trajectory. In this respect, (3) is an optimal *kinematic* approximation of the reference.

The standard [2] dynamic model for the Fourier coefficients is *Galerkin projection* of the NSE onto the subspace spanned by (3) ,

$$\frac{d}{dt} a_i = \frac{1}{Re} \sum_{j=0}^{N} l_{ij} \, a_j + \sum_{j,k=0}^{N} q_{ijk} \, a_j \, a_k \quad \text{for } i = 1, \dots, N, \quad (4)$$

where the linear and quadratic terms represent the viscous and convective Navier-Stokes terms, respectively, with constant coefficients $l_{ij} := (\mathbf{u}_i, \triangle \mathbf{u}_j)_\Omega$, $q_{ijk} := (\mathbf{u}_i, \nabla \cdot (\mathbf{u}_j, \mathbf{u}_k))_\Omega$. The pressure term may change the coefficients q_{ijk}, but not the form (4) [7].

The reference data and corresponding GM may describe a natural or forced flow. Forcing may enhance coherent structures and thus reduce the attractor's GM dimension. Examples are the 4-dimensional model of Kelvin-Helmholtz vortices of a shear-layer [7] excited by periodic inlet condition and the 32-dimensional model of a transitional boundary layer, manipulated by a periodic upstream tripping wire [3]. The key issue is that the standard POD approximation is hardwired to the reference, including a specific actuation, and the Galerkin system (GS) has no free actuation input. This excludes the standard Galerkin modeling approach for control design.

B. Shift-mode

The shift-mode $\mathbf{u}_\Delta \propto \mathbf{u}_0 - \mathbf{u}_s$ is a mean-field correction (where $\mathbf{u}_s$ is the unstable steady NSE solution) and is orthogonal to the POD modes. Including the shift-mode $\mathbf{u}_\Delta$ as the $N+1^{st}$ mode in (3) is an enabler for non-equilibrium model for transient flow [8], [9], [13].

C. Volume force representation

The volume force in the NSE (1) may represent, e.g., a Lorentz force in magneto-hydrodynamical flows, a buoyancy term in the Boussinesq approximation, or an external pressure gradient in pipe flows. The control command, $\epsilon(t)$, modulates the fixed field $\mathbf{g}(\mathbf{x})$. This corresponds to a control term of the form $\epsilon \, g_i$ on the right-hand side of the ith GS equation (4), where $g_i := (\mathbf{u}_i, \mathbf{g})_\Omega$ is the magnitude of the projection of $\mathbf{g}$ on $\mathbf{u}_i$. This basic textbook form of actuation is chosen for nomenclature simplicity. Alternative forcing may involve state dependent g_i coefficients [18].

III. MODEL-BASED STABILIZATION OF THE CYLINDER WAKE

A. The System and a Simple Complete Information Control

The circular cylinder wake flow transition to instability and vortex shedding, forming a periodic attractor, at $Re \approx 47$, and is considered here at $Re = 100$. Figure 1 is a schematic of a planar flow with two forms of actuation: The vertical volume-force actuator used in this note, and an AFA experimental rig with vertical vibrations of the disk, as in [10], [11], [18]. Streamlines represent the natural flow. Optimized sensor(s) position are discussed in §III-F.

Vortex shedding is undesirable, as it causes mechanical vibrations and drag, and the design objective is the attenuation and delay of shedding to the far wake. A physically motivated control policy is based on *dissipation*: the *energy extraction rate* $-\epsilon(t)(\mathbf{g}, \mathbf{u}(t))_\Omega \approx -\epsilon(t)v_{vf}(t)A_g$, where v_{vf} and A_g are the respective vertical velocity field at the center of the supporting disk of the volume force, and the area of that disk. This gives rise to the feedback $\epsilon = -k(\mathbf{g}, \mathbf{u})_\Omega \approx -k \, A_g \, v_{vf}$, where the gain $k > 0$ determines the dissipation rate. Indeed, implementing this policy directly on the DNS model can be shown to completely attenuate vortex shedding.

B. A Standard POD Model of the Cylinder Wake

The natural attractor is dominated by two modes - $\mathbf{u}_1$ and $\mathbf{u}_2$ in Figure 2 - capturing some 95% of the perturbation energy. The structurally similar mean flow $\mathbf{u}_0$ (same figure) and the unstable, steady flow $\mathbf{u}_s$, are characterized by symmetry with respect to the x axis and a near wake recirculation bubble which becomes shorter during transition to the attractor. The normalized difference $\mathbf{u}_0 - \mathbf{u}_s$ is the shift mode $\mathbf{u}_\Delta = \mathbf{u}_3$. (Thus the Fourier coefficient value $a_3 = 0$ represents the attractor.) The respective GS is of the form

$$\dot{a} = A(a)a + B\epsilon + \eta, \quad s = Ca \quad (5)$$

where $a := [a_1, a_2, a_3]^T$, $\eta = [0, 0, \eta_3]^T$ is the constant term from (4), ϵ is the actuation command, s is the sensor signal, and

$$A(a) := \begin{bmatrix} \sigma_r & -(\omega + \gamma a_3) & -\beta a_1 \\ (\omega + \gamma a_3) & \sigma_r & -\beta a_2 \\ \delta a_1 & \delta a_2 & -\rho \end{bmatrix}, \quad B = \begin{bmatrix} g_1 \\ g_2 \\ 0 \end{bmatrix} \tag{6}$$

This form[1] clearly reveals the key features of a periodic attractor and a nearly parabolic attractive invariant manifold, formed by transients from perturbations of the steady solution ($a_1 = a_2 = 0$, $a_3 = -\eta_3/\rho$) to the attractor ($a_3 = 0$), in the unactuated flow [8], [17].
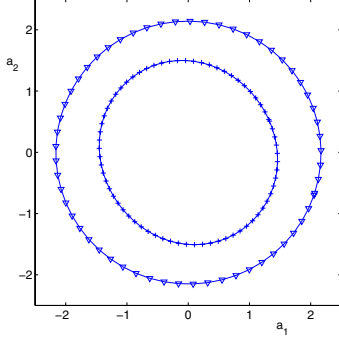

Fig. 3. Phase portrait of the first two Fourier coefficients a_1, a_2. The outer limit cycle represents the periodic natural flow, the inner limit cycle the optimally actuated flows. Both attractors are obtained from a direct numerical simulation (DNS) and projected on the natural POD modes.

C. Control Design with POD of the Natural Flow

A basic and critical observation concerning model based flow control, is that the actuated flow should remain within the dynamic validity envelope of the models, to avoid unpredictable, ineffective and possibly altogether counter productive response to actuation. This may include the need to maintain the natural oscillation frequency and slow amplitude variations [12], [13]. The flip side of these restrictions, utilized below, is a relatively simple actuation and observer structure.

Key aspects of actuation restrictions are clarified when (6) is expressed in cylindrical coordinates $[a_1, a_2]^T = [\cos(\phi), \sin(\phi)]^T r$:

$$\begin{bmatrix} \dot{r} \\ \dot{a}_3 \end{bmatrix} = \begin{bmatrix} \sigma_r & -\beta r \\ \delta r & -\rho \end{bmatrix} \begin{bmatrix} r \\ a_3 \end{bmatrix} + b \begin{bmatrix} \cos(\theta - \phi) \\ 0 \end{bmatrix} \epsilon + \begin{bmatrix} 0 \\ \eta_3 \end{bmatrix} \tag{7}$$

$$\dot{\phi} = \omega + \gamma a_3 + \frac{b}{r} \sin(\theta - \phi)\epsilon \tag{8}$$

where $\theta = \angle(g_1, g_2)$ and $b = \sqrt{g_1^2 + g_2^2}$. This form reveals two basic facts: First, *however designed*, an admissible and effective attenuating actuation must be in phase with $-\cos(\theta - \phi)$ [9], [12], [13]. That is, such control policy is bound to (roughly) immitate the simple physics based, dissipative policy suggested in §III-A. A subsequent observation is that the angle θ, extracted from the low dimensional Galerkin approximation, is critical to correct orientation of the actuation force. This point will be revisited later.

A simple GM based counterpart of the dissipative control of §III-A is that where the inner product $(\mathbf{g}, \mathbf{u}(t))_\Omega$ is substituted by the Galerkin approximation: Since the mean flow makes no contribution to the vertical velocity along $x = 0$, the Galerkin approximation (3) leads to $a_1(t)g_1 + a_2(t)g_2$. *Equivalently*, the actuation is set to be proportional to $-br\cos(\theta - \phi)$. A dynamic observer [9], [12] could be used to dynamically estimate the Fourier coefficients, hence the values of r and ϕ, from sensor data (ignoring here the

[1]The convention that $a_3 = 0$ on the attractor is different from some of our previous notes, and results here with $\sigma_r \approx 0$.

trivial case where fluid velocity could be sensed directly at the point of actuation). Fig. 3 compares the natural limit cycle and the feasible attenuated limit cycle in terms of periodic orbits of a_1 and a_2. Data were obtained by DNS simulations (i.e., of the NSE (1)) and a_i were computed by projection of the simulated flow field on $\mathbf{u}_i$ (i.e., this is a "complete information" GM-based control).

D. Interpolated POD Models

The limited scope of control based on a POD model extracted from the natural attractor is due to the declining ability of that model to represent the flow, as vortex shedding is attenuated. To understand this phenomenon it is useful to consider Figure 2 (b), (c) and (d). These plots are based on three sets of simulations: The natural attractor and two controlled limit cycles, obtained by the physics based control of §III-A with a moderate and a more aggressive feedback gains: Figure 2 column (b) depicts snapshots of the respective flow fields and the plots in columns (c) and (d), the corresponding mean flow fields and the first oscillatory POD modes. The emerging observation is that, while the topological characteristics of all three flow conditions are similar, they do demonstrate significant mutual deformations: As the flow is increasingly stabilized, the recirculation bubble is gradually elongated and the coherent flow structures formed by shed vortices are pushed downstream. Quantitative features of the corresponding Galerkin systems (noted already in the context of natural transients from the steady flow to the attractor [8]) include variations in the oscillation period (which grows as the dominant modes stretch in space) and in the local growth rate. Particularly relevant here are well expected significant differences between the projections of the volume force on the three modes in Figure 2 (d), hence differences between the respective values of the all critical angle θ. Figure 4 illustrates this distortive effect on phase prediction along a stabilized trajectory. The ideal actuation phase (horizontal bold line) for an operating point on an attenuated (forced) attractor is compared with the phase predicted by POD modes obtained from both the natural attractor and a set of forced attractors. The horizontal axis stands for the actuation level of the respective attractor, where 0 relates to the natural attractor and 1 for the nearly attenuated vortex shedding. The 4 curves stand for phases computed with POD modes from four computational domain lengths, of 4, 6, 8 and 15 cylinder diameters downstream. The GM predicted phase coincides (here, by all curves) with the correct phase when the used POD are from the forced limit cycle nearest to the selected flow snapshot. Yet the use of other models, in particular the POD of the natural attractor, yield erroneous results.

Consequently, when POD modes from the wrong orbit are used, the evaluated θ is distorted, and if actuation is based solely on the POD modes from the natural attractor, the distortion in θ rapidly reaches a level that makes the attenuating force and associated observers, ineffectual, limiting the scope of such a policy [25]. Indeed, this is the limiting factor of the attenuation depicted in Figure 3. A second and related observation is that the quality of the approximation of the flow field deteriorates as the flow departs from the natural attractor. Thus, the radius of the controlled cycle in Figure 3 under-predicts the perturbation energy in the actual flow and over predicts the attenuating effect of that feedback policy.

The solution suggested in this note aims to exploit the structural similarity between controlled limit cycles, representing intermediate points between the natural attractor and the steady flow, and at the same time, compensate for the differences between them: The controlled limit cycles, represented by the several lightly doted
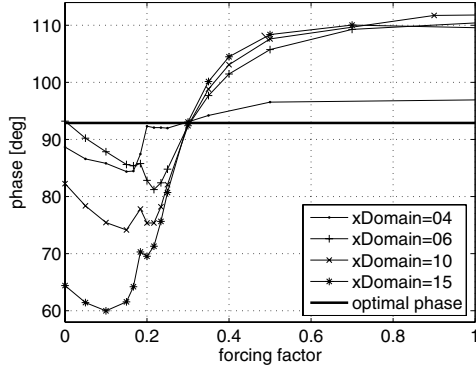
Fig. 4. The ideal actuation phase (horizontal bold line) for an operating point on an attenuated (forced) attractor, compared with the phase predicted by POD modes from a set of attractors. The horizontal axis stands for the POD mode set, where 0 relates to the natural attractor and 1 for the nearly attenuated vortex shedding. The 4 curves stand for POD modes from four computational domain lengths of 4, 6, 8 and 15 cylinder diameters downstream. The GM predicted phase coincides with the correct phase when the used POD are from the forced limit cycle nearest to the selected flow snapshot. Yet the use of other models, including the POD of the natural attractor, yield erroneous results.

circles in Figure 6, were obtained by complete information feedback $\epsilon = -kv_{vf}$, for escalated values of the gain k. We are interested in transients along the manifold connecting these cycles. The dynamics near each of the cycles is dominated by the (same) shift mode and two locally extracted oscillatory modes $\mathbf{u}_1$ and $\mathbf{u}_2$. The Galerkin systems obtained by projecting the NSE (1) on these local modes are each of the form (6)-(8), albeit with different coefficients, which could be parameterized by the characteristic value of a_3 on the respective cycle. That is, the local values of β, δ, ω, γ, ρ, η_3, g_1 and g_2, are functions of the characteristic value a_3 (equiv. of the respective length x_{Rec} of the recirculation bubble). This dependence can be easily parameterized or tabulated. If, in addition, the local $\mathbf{u}_1$ and $\mathbf{u}_2$ modes or oriented so that the local Fourier coefficients a_1 and a_2 of a flow field will transition continuously between neighboring models, a global interpolated model will be formed: It will retain the form (6) (with a_3 dependent coefficients) and the Fourier coefficients will be interpreted with respect to the local expansion modes that is associated with a_3. This model will be valid for slow vertical transitions along the dynamic manifold in Figure 6 (which prevents the need to include the dynamics of mode deformation). While the total number of modes used in constructing the interpolated model may be large, say, on par with the number of modes used in [20], the great advantage of the proposed model is that, at any given time, only a small number of Fourier coefficients - here 3 coefficients - are involved. The Galerkin system thus maintains a relatively simple, low dimensional structure. These advantages make the interpolated model particularly suitable for practical feedback design and implementation.

While the technical details of the interpolation deserve well more than the space available here, the key relevant fact for control design, in our system, is that the local model provides both the appropriate value of $\theta := \angle(g_1, g_2)$ and appropriate local concepts of the instantaneous phase ϕ and amplitude r, of the flow. Indeed, these are the three key quantities needed for effective control.

E. Control Design With Interpolated POD Models

Demonstrating the advantage of the suggested modeling paradigm for control design, we implement the counterpart of the physics based control of §III-A, now, using the interpolated Galerkin

model to estimate v_{vf} in terms of the Fourier coefficients a_1 and a_2, as determined by the current local model. (Equiv., we extract local values of r, ϕ and θ.) The dissipative control policy remains $\epsilon = -kv_{vf}$ (equiv., $\epsilon = -\tilde{k}r\cos(\theta - \phi)$). Figure 6 compares the natural attractor with limit cycles obtained by feedback control with a POD model extracted from the natural flow, control using the interpolated Galerkin model, and, as a benchmark, control with direct flow measurement. In all cases, the control policy and feedback gain are identical: $k = 0.3$. As can be seen, the attenuation achieved with the traditional POD model is much inferior to what is attained with the interpolated model, which, in turn is close to the response with direct flow measurement. This improvement is enabled by the fact that the high level of flow reconstruction by the interpolated model is maintained along trajectories, but lost when the natural attractor's POD is used.

In closing this section it must be noted that the simplicity of low order description need not mask the intrinsic distributed nature of the flow. Here, holding transients on the targeted manifold becomes harder as vortex shedding is attenuated. The reason is the relative weight of the flow field within the volume force domain is approaching zero, making phase prediction especially difficult. Figure 5 depicts the trajectories of a GM based forcing and of the inner product $(\mathbf{g}, \mathbf{u})_\Omega$, as well as representation of the phase prediction at two representative snapshots of that flow trajectory. As the flow field over the volume force domain attenuates, closed loop dynamics develops a periodic "ringing", whereby the correct phase prediction deteriorates as the $(\mathbf{g}, \mathbf{u})_\Omega$ approaches zero and is recovered when oscillations increase. As can be anticipated, the best phase predictions are associated with POD modes obtained on the shortest domain, which offers the tightest cover of the volume force.

F. Optimizing Sensor Location and Observation with an Interpolated POD Model

As in any feedback design, dynamic observers / estimators are intrinsic in closed loop flow control. The challenges posed by the distributive nature of the flow and the often strict physical limitations on hardware (i.e., space, weight, location, etc.) are as manifest in this context as they are in the context flow actuation. The viability of observer based feedback in the current system has been demonstrated in [9], [12]. Here we shall therefore be content with brief comments concerning observer design, and dedicate the remaining available space to the benefits of the interpolated model in optimizing sensor location(s).

In the context of the dissipative actuation, above, an observer is charged with two tasks: The estimation of the "vertical" flow state position along the manifold depicted in Figure 6, and, given that evaluation, the estimation of the Fourier coefficients, relative to the appropriate local Galerkin expansion. As long as actuation does not impose sharp "vertical" transients, the former task amounts to a determination of a_3 (relative to the unique shift mode) or an equivalent quantity. Examples of equivalent quantities include the oscillation amplitude and frequency [9], which stand in a monotonous relation with a_3. When the controlled changes in the operating condition, hence the frequency, are slow, the frequency can be easily tracked in real time from oscillatory sensor readings [26] whose primary targets are the Fourier coefficients a_1 and a_2, as detailed below. An alternative is the low pass filtered version of a stream-wise velocity sensor reading. A good location to minimize the harmonic component would be along the equator, downstream from the saddle point $(x_{\mathrm{Rec}}, 0)$, say at $(5, 0)$. As seen in Figure
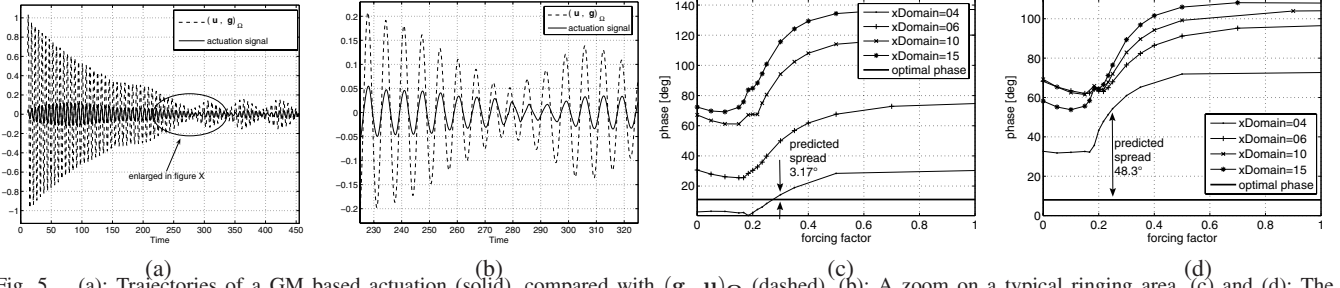
Fig. 5. (a): Trajectories of a GM based actuation (solid), compared with $(\mathbf{g}, \mathbf{u})_\Omega$ (dashed). (b): A zoom on a typical ringing area. (c) and (d): The GM predicted actuation phase (same convention as Figure 4) compared with the correct phase for two snapshots from the zoomed area. Best prediction is always obtained with POD modes from the shortest domain.
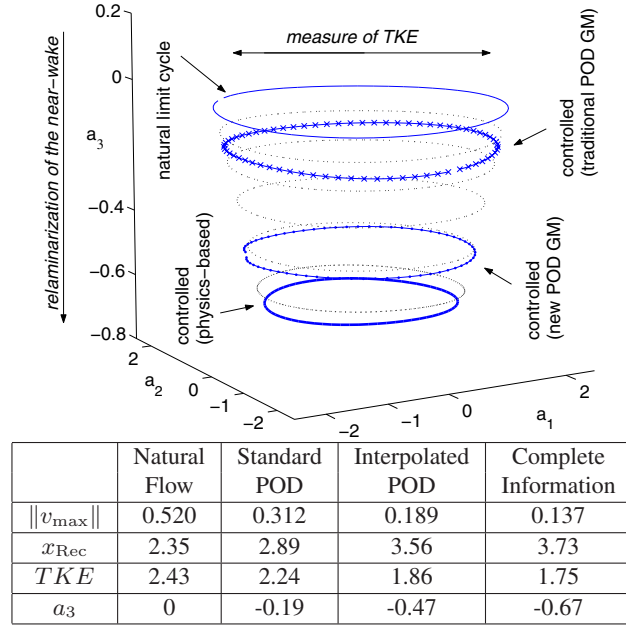

	Natural Flow	Standard POD	Interpolated POD	Complete Information
$\|v_{\max}\|$	0.520	0.312	0.189	0.137
x_{Rec}	2.35	2.89	3.56	3.73
TKE	2.43	2.24	1.86	1.75
a_3	0	-0.19	-0.47	-0.67

Fig. 6. Top: Phase portrait of the first three Fourier coefficients a_1, a_2, a_3, obtained by projecting direct numerical simulations of the NSE (1) on the respective base modes. Four limit cycles are shown: i) the natural flow, ii) the actuated flow with a standard POD Galerkin model (GM), iii) the actuated flow with the interpolated POD GM, and iv) the dissipative feedback with direct flow measurements, all with $\epsilon = -0.3 v_{vf}$. The dotted black circles are limit cycles of under lower gain dissipative control. Together, these represent sections of the manifold associated with actuated transients. Bottom: Tabulated quantities related to the plot, including: a) the oscillation amplitude of the (actual) vertical velocity v_{vf} at the center of the volume force, denoted $v_{vf\,\max}$, b) the average length of the recirculation bubble x_{Rec}, c) the perturbation (= turbulent kinetic) energy (TKE) in each limit cycle, and d) the Fourier coefficient a_3.

7, this quantity provides a good indicator of both the operating condition (hence of a_3) and of the associated oscillation frequency.

Under slow transition in the operating condition (hence in a_3 and r) the dynamic estimation of the Fourier coefficients becomes equivalent to observer design in a pure oscillator with slow drifts in its periodic characteristics. The main task is then phase estimation, rather than full state estimation as in [9], [12]. We shall use this framework as a simple illustration of issues associated with optimizing sensor(s) location.

A simplified dynamic model is then

$$\frac{d}{dt}\begin{bmatrix} a_1 \\ a_2 \end{bmatrix} = \begin{bmatrix} 0 & -\bar{\omega} \\ \bar{\omega} & 0 \end{bmatrix}\begin{bmatrix} a_1 \\ a_2 \end{bmatrix}, \qquad s = C\begin{bmatrix} a_1 \\ a_2 \end{bmatrix} \qquad (9)$$

where $\bar{\omega}$ is the (known) instantaneous frequency, the known con-
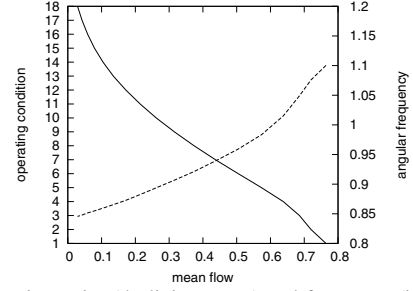

Fig. 7. Operating point (declining curve) and frequency (inclining curve) as functions of the mean flow at $(5, 0)$.

tribution of a_3 has been removed from the sensed velocity (or velocities) signal s, and terms associated with the slow net amplitude growth or decay are neglected. Given a set of m velocity sensors, the entries of the two columns of C are

$$C_{i,j}(\lambda, p) = \mathbf{v}_i^T \mathbf{u}_j(\mathbf{x}_i), \qquad i = 1, \ldots, m, \quad j = 1, 2$$

where λ parameterizes the operating conditions, p parameterizes the set of sensor locations $\mathbf{x}_i$ and respective orientation unit vectors $\mathbf{v}_i$. A good indicator of the sensitivity of the sensors to the state is the *Observability Grammian*. Since we are interested in short time behavior of a system with a drift, we shall consider the normalized finite time Grammian over a period $\bar{T} = 2\pi/\bar{\omega}$:

$$G = \frac{1}{\bar{T}}\int_0^{\bar{T}} e^{A't}C'Ce^{At}dt = \frac{1}{2}\|C\|_F^2 I_2 \qquad (10)$$

where we use the "A" matrix from (9), $\|C\|_F$ is the Frobinius norm, I_2 is the identity matrix, and where the second equality is obtained by straightforward calculation. Having fixed λ, an optimal sensor placement is thus one that maximizes $\|C\|_F$. This issue has already been addressed in the cylinder wake benchmark [27], albeit based on the physical insight that it is advantageous to place and orient velocity sensors at points of local extrema of $\mathbf{u}_1$ and $\mathbf{u}_2$, rather than on Grammian evaluation.

The true issue, however, is due to the location of such extrema varying markedly with the operating point, as easily predicted from Figure 2 (b), (c) and (d). A meaningful criterion is thus rather to maximize the worst case value of G, over all operating points:

$$\max_p \min_\lambda \|C(\lambda, p)\|_F^2 \qquad (11)$$

The optimal set of sensors is defined by p_* for which the maximum in (11) is attained. This is dependent, of course, on the range of operating conditions considered.

In Figure 8 we show plots of $\|C(\lambda, p)\|_F^2$ as a function of λ, where p was optimized with respect to the first 1, 4, 9 or 18 (out of 18) equally spaced operating conditions, and for the case of a single and for three velocity sensors. As is clearly

observed, the performance of sensors that are selected for a single λ (i.e., for the natural attractor) is higher early on but deteriorates rapidly with the change of λ, while those optimized over a wider range maintain an increasingly even performance during transitions. Multiple sensors improve the relative flatness (peak-to-peak ratio) of this performance measure.
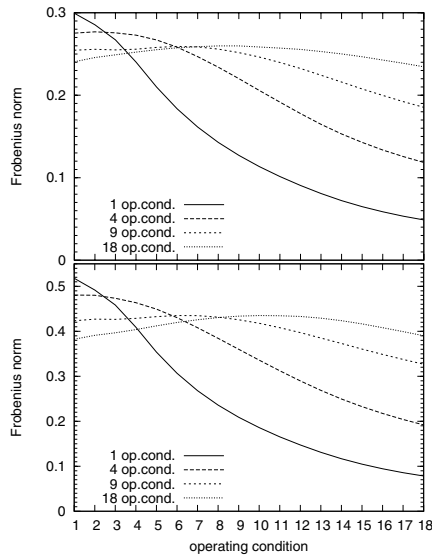

Fig. 8. Plots of $\|C(\lambda, p_*)\|_F$ as a function of λ for a single sensor (top) and 3 sensors (bottom). The optimal sensor location(s) vector p_* is computed for the first 1, 24, 9 or 18 (out of 18) equally spaced operating points.

IV. CONCLUSIONS

A framework of interpolated Galerkin models for fluid flow systems strikes a balance between the need for higher number of modes to represent actuation and transients and the desire to maintain model simplicity and minimize the number of dynamic variables that need to be estimated in real time, in feedback implementation. Advantages over traditional POD models have been illustrated in the context of vortex shedding suppression behind a circular cylinder, and are manifest by improved ability to suppress vortex shedding and an improved sensor performance over a wider transients range.

REFERENCES

[1] T. R. Bewley. Flow control: new challenges for a new renaissance. *Progress in Aerospace Sciences*, 37:21 – 58, 2001.

[2] P. Holmes, J. L. Lumley, and G. Berkooz. *Turbulence, Coherent Structures, Dynamical Systems and Symmetry*. Cambridge University Press, 1998.

[3] D. Rempfer. *Kohärente Strukturen und Chaos beim laminar-turbulenten Grenzschichtumschlag*. PhD thesis, Fakultät Verfahrenstechnik der Universität Stuttgart, 1991.

[4] J.L. Lumley and P.N. Blossey. Control of turbulence. *Ann. Rev. Fluid Mech.*, 30:311–327, 1998.

[5] S.S. Ravindran. Adaptive reduced-order controllers for a thermal flow system. *SIAM Journal on Scientific Computing*, 23:1924–1942, 2002.

[6] O.K. Rediniotis, J. Ko, and A.J. Kurdila. Reduced order nonlinear Navier-Stokes models for synthetic jets. *J. Fluids Enrng.*, 124(2):433–443, 2002.

[7] B.R. Noack, P. Papas, and P.A. Monkewitz. The need for a pressure-term representation in empirical Galerkin models of incompressible shear flows. *J. Fluid Mech.*, 523:339–365, 2005.

[8] B.R. Noack, K. Afanasiev, M. Morzyński, G. Tadmor, and F. Thiele. A hierarchy of low-dimensional models for the transient and post-transient cylinder wake. *J. Fluid Mech.*, 497:335–363, 2003.

[9] J. Gerhard, M. Pastoor, R. King, B.R. Noack, A. Dillmann, M. Morzyński, and G. Tadmor. Model-based control of vortex shedding using low-dimensional Galerkin models. In *33rd AIAA Fluids Conference and Exhibit*, Orlando, Florida, U.S.A., June 23–26, 2003, 2003. Paper 2003-4262.

[10] K. Cohen, S. Siegel, T. McLaughlin, and J. Myatt. Proper orthogonal decomposition modeling of a controlled Ginzburg-Landau cylinder wake model. In *41st Aerospace Sciences Meeting and Exhibit, Reno NV*, 2003.

[11] S. Siegel, K. Cohen, and T. McLaughlin. Feedback control of a circular cylinder wake in experiment and simulation. In *33rd AIAA Fluids Conference and Exhibit*, Orlando, Florida, U.S.A., June 23–26, 2003, 2003. Paper No 2003-3571.

[12] G. Tadmor, B.R. Noack, A. Dillmann, J. Gerhard, M. Pastoor, R. King, and M. Morzyński. Control, observation and energy regulation of wake flow instabilities. In *42nd IEEE Conference on Decision and Control 2003*, pages 2334–2339, Maui, HI, U.S.A., 9.-12. December 2003, 2003. WeM10-4.

[13] R. King, M. Seibold, O. Lehmann, B.R. Noack, M. Morzyński and G. Tadmor. Nonlinear flow control based on a low dimensional model of fluid flow. In *Control and Observer Design for Nonlinear Finite and Infinite Dimensional Systems*. Lecture Notes in Control and Information Sciences, LNCIS, Vol. 322, T. Meurer, K. Graichen, E.D. Gilles (Eds.), pp.351-368, Springer, 2005.

[14] L. Cordier and M. Bergmann. Proper Orthogonal Decomposition: An Overview. *VKI Lecture Series 2003-04*. Von Kármán Institut for Fluid Dynamics, 2003.

[15] K. Cohen, S. Siegel, M. Luchtenburg, T. McLaughlin, and A. Seifert. Sensor placement for closed-loop flow control of a 'D' shaped cylinder wake. In *2nd AIAA Flow Control Conference*, Portland, Oregon, U.S.A., 28.6.–1.7.2004, 2004. Paper 2004-2523.

[16] C.W. Rowley, T. Colonius, and R.M. Murray. Model reduction for compressible flows using POD and Galerkin projection. *Physica D*, 189:115–129, 2004.

[17] G. Tadmor and B.R. Noack. Dynamic estimation for reduced Galerkin models of fluid flows. In *The 2004 American Control Conference*, Boston, MA, U.S.A., June 30–July 2, 2004, 2004. Paper **WeM18.1**.

[18] B.R. Noack, G. Tadmor, and M. Morzyński. Actuation models and dissipative control in empirical Galerkin models of fluid flows. In *The 2004 American Control Conference*, Boston, MA, U.S.A., June 30–July 2, 2004, 2004. Paper **FrP15.6**.

[19] C.W. Rowley. Model reduction for fluids, using balanced proper orthogonal decomposition. *Int. J. on Bifurcation and Chaos*, 2005. in press.

[20] M. Bergmann, L. Cordier, and J.-P. Brancher. Optimal rotary control of the cylinder wake using POD reduced order model. In *2nd AIAA Flow Control Conference*, Portland, Oregon, U.S.A., 28.6.–1.7.2004, 2004. Paper 2004-2323.

[21] M. F. Unal and D. Rockwell. On the vortex formation from a cylinder; Part 2. control by a splitter-plate interference. *J. Fluid Mechanics*, 190:513–529, 1987.

[22] P. J. Strykowski and K. R. Sreenivasan. On the formation and suppression of vortex shedding at low Reynolds numbers. *J. Fluid Mechanics*, 218, 1990.

[23] E. Detemple-Laake and H. Eckelmann. Phenomenology of Kármán vortex streets in oscillatory flow. *Exps. Fluids*, 7:217–227, 1989.

[24] K. Roussopoulos. Feedback control of vortex shedding at low Reynolds numbers. *J. Fluid Mechanics*, 248:267–296, 1993.

[25] J. Gerhard, M. Pastoor, R. King, B. R. Noack, A. Dillmann, M. Morzyński, and G. Tadmor. Model-based control of vortex shedding using low-dimensional Galerkin models. In *Proc. AIAA Fluid Dynamics Conference and Exhibit*, Orlando, Florida, June 23–26, 2003. Paper 2003-4261.

[26] G. Tadmor. Observers and feedback control for a rotating vortex pair. *IEEE Transactions on Control Systems Technology*, 12:36 – 51, 2004.

[27] K. Cohen, S. Siegel, and T. McLaughlin. Sensor placement based on proper orthogonal decomposition of a cylinder wake. In *33rd AIAA Fluids Conference and Exhibit*, Orlando, Florida, U.S.A., June 23–26, 2003. Paper No 2003-4259.